Micromagnetic Modeling on Magnetisation Dynamics with Lossy Magnetic Material in Thin Film Heads by FDTD Calculations

Gustavo Recio and César Estébanez

Department of Computer Science
Universidad Carlos III de Madrid, Spain
grecio@inf.uc3m.es, cesteban@inf.uc3m.es

***Abstract* —** An extension to the standard FDTD formulation aimed at modelling the micromagnetics of materials together with the solution of Maxwell's equations is presented in this paper. Numerical computations using actual thin film head geometries were carried out with the purpose of validating the method. The analysis of results revealed the importance of the method for modelling electromagnetic interaction with lossy magnetic material in the presence of current and magnetic sources.

***Index Terms* —** FDTD Computations, Equation of Motion, Eddy Currents, Magnetic Losses, Micromagnetic Model, Recording Heads, Magnetic Recording, Thin Film Heads.

I. INTRODUCTION

Advances in recording speeds have reached a point where the micromagnetics of the heads have become a physical limit. Consequently, to continue with the rise in areal storage densities and to push towards higher recording speeds, research has been focused on understanding and improving flux propagation and reversal times in thin-films inductive recording heads [1], [2]. The flux reversal time is the time required in order to obtain a response from the magnetic flux (inside the head circuit) to changes in the write current waveform. Minimising this time in the head yoke reduces the rise time of the writing fields in the pole tip region and allows shorter and well defined magnetic transitions to be written onto the storage medium [3].

High-speed experimental studies using the time-resolved magneto-optical Kerr microscope on magnetic thin-films [1] and on thin-film recording heads [2] have contributed to furthering the understanding of the switching mechanisms in these magnetic structures. With the reduction of the size of the active regions in thin-film recording heads [4], the ability to observe the flux distribution during switching in the pole tip region of heads is becoming beyond the optical resolution of this technique. As a result, modelling and simulation are becoming increasingly important as alternative tools to understand the flux reversal process in these small head features and to enable the optimisation of write head designs. This motivated the study of the contribution and effect of eddy currents when working at high frequencies, e.g. developing non-destructive evaluations of conductive materials by means of eddy current imaging [5].

Static models of characterising magnetic heads include equivalent circuit models, transmission line models and finite elements models [6], [7], [8], [9], [10], [11]. These are either time independent or limited in the frequency domain to the fundamental response, and ignore the magnetic detail of the head material. Dynamic models, on the other hand, utilise full micromagnetic description of the magnetic material [12], but the absence of electromagnetic formulation in these models neglects the eddy current effect coming from time varying fields in the finite resistivity thin-film materials. Therefore the need arises for a dynamic model that combines the solution to Maxwell's equations for the electromagnetic fields with micromagnetic models of the material to accurately simulate the reversal process in magnetic heads.

Modern computational methods such as the Finite Difference Time Domain (FDTD) algorithm will play a key role in modelling magnetic heads in the future [13]. The FDTD method solves the electromagnetic phenomena for a given geometry inside a computational space and, as a result, the magnitude and direction of the electromagnetic fields are given for the whole computational space. This research extends

Submitted On: March 1, 2012
Accepted On: July 22, 2012

the standard FDTD algorithm to model the micromagnetics of materials together with the solution of Maxwell's equations having in this manner a better description of the reversal process. Studying and characterising the fast switching process (dynamics) in thin-film heads is the main aim of this work which will be achieved through FDTD computations of actual thin-film head geometries. The advantage provided by this study is that magnetisation motion can be simulated considering electromagnetic interaction in lossy magnetic material by making use of the FDTD method and the LLG equation (having a better description of the reversal process).

This paper is organised as follows, Section II formalises the general electromagnetic theory and the micromagnetic model formulation for non-linear magnetic materials which form the basis behind the numerical work in this research. Section III presents the discretisation of the equation of motion. Space and time synchronism, boundary conditions and stability of the extended method are dealt with in Sections IV, V and VI respectively. In Section VII the numerical experiments carried out are presented followed by an analysis of results. The paper concludes with a discussion of the main findings in Section VIII.

II. Non-linear Magnetic Materials

When linear magnetic materials are considered, the magnetic flux density $\mathbf{B}$ is proportional to the external magnetic field $\mathbf{H_{app}}$ by a constant called the permeability of the material μ. However, when considering non-linear magnetic materials, the following equation applies

$$\mathbf{B} = \mu_o(\mathbf{H_{app}} + \mathbf{M}) \tag{1}$$

where the magnetisation vector $\mathbf{M}$ is taken into account to calculate the magnetic flux density.

Extending the FDTD method to non-linear magnetic materials requires to start by considering Maxwell's curl equations for a general medium.

$$\frac{\partial \mathbf{B}}{\partial t} = -\nabla \times \mathbf{E} \tag{2}$$

$$\frac{\partial \mathbf{D}}{\partial t} = \nabla \times \mathbf{H_{eff}} \tag{3}$$

where $\mathbf{B}$ is as in (1) and

$$\mathbf{D} = \epsilon \mathbf{E} \tag{4}$$

substituting $\mathbf{B}$ and $\mathbf{D}$ into (2) and (3) yields

$$\frac{\partial \mathbf{H_{app}}}{\partial t} = -\frac{1}{\mu_o}\nabla \times \mathbf{E} - \frac{\partial \mathbf{M}}{\partial t} \tag{5}$$

$$\frac{\partial \mathbf{E}}{\partial t} = \frac{1}{\epsilon}\nabla \times \mathbf{H_{eff}} \tag{6}$$

where the nonlinearity introduced by the term $\partial\mathbf{M}/\partial t$ is described by Landau-Lifshitz-Gilbert's (LLG) equation [14].

$$\frac{\partial \mathbf{M}}{\partial t} = -\gamma(\mathbf{M} \times \mathbf{H_{eff}}) + \frac{\alpha}{M_s}\left(\mathbf{M} \times \frac{\partial \mathbf{M}}{\partial t}\right) \tag{7}$$

III. Discretisation of LLG Equation

To discretise all of above equations, central finite difference expressions, which provide second order accuracy, for the space and time derivatives are used. Equation (6) follows the same expression as in the normal FDTD method therefore no changes are needed for the E_z component in the 2D TM_z mode.

$$\begin{aligned} E_z|^{n+\frac{1}{2}}_{i+\frac{1}{2},j+\frac{1}{2}} &= C_a|_{i+\frac{1}{2},j+\frac{1}{2}} E_z|^{n-\frac{1}{2}}_{i+\frac{1}{2},j+\frac{1}{2}} \\ &+ C_b|_{i+\frac{1}{2},j+\frac{1}{2}} \Big(H_y|^n_{i+1,j+\frac{1}{2}} - H_y|^n_{i,j+\frac{1}{2}} \\ &+ H_x|^n_{i+\frac{1}{2},j} - H_x|^n_{i+\frac{1}{2},j+1} \Big) \end{aligned} \tag{8}$$

Equation (5) has a new term $\partial M/\partial t$, which is discretised using central differences in time, and it must be included in the final expressions for H_x and H_y.

$$\begin{aligned} H_x|^{n+1}_{i+\frac{1}{2},j+1} &= D_a|_{i+\frac{1}{2},j+1} H_x|^n_{i+\frac{1}{2},j+1} \\ &+ D_b|_{i+\frac{1}{2},j+1} \Big(E_z|^{n+\frac{1}{2}}_{i+\frac{1}{2},j+\frac{1}{2}} - E_z|^{n+\frac{1}{2}}_{i+\frac{1}{2},j+\frac{3}{2}} \Big) \\ &- M_x|^{n+1}_{i+\frac{1}{2},j+1} + M_x|^n_{i+\frac{1}{2},j+1} \end{aligned} \tag{9}$$

$$\begin{aligned} H_y|^{n+1}_{i+1,j+\frac{1}{2}} &= D_a|_{i+1,j+\frac{1}{2}} H_y|^n_{i+1,j+\frac{1}{2}} \\ &+ D_b|_{i+1,j+\frac{1}{2}} \Big(E_z|^{n+\frac{1}{2}}_{i+\frac{3}{2},j+\frac{1}{2}} - E_z|^{n+\frac{1}{2}}_{i+\frac{1}{2},j+\frac{1}{2}} \Big) \\ &- M_y|^{n+1}_{i+\frac{1}{2},j+1} + M_y|^n_{i+\frac{1}{2},j+1} \end{aligned} \tag{10}$$

where the coefficients C and D are described as

$$C_a|_{i,j} = \left(1 - \frac{\sigma_{i,j}\Delta t}{2\varepsilon_{i,j}}\right) \Big/ \left(1 + \frac{\sigma_{i,j}\Delta t}{2\varepsilon_{i,j}}\right) \tag{11}$$

$$C_b|_{i,j} = \left(\frac{\Delta t}{\varepsilon_{i,j}}\Delta\right) \Big/ \left(1 + \frac{\sigma_{i,j}\Delta t}{2\varepsilon_{i,j}}\right) \tag{12}$$

$$D_a|_{i,j} = \left(1 - \frac{\sigma^*_{i,j}\Delta t}{2\mu_{i,j}}\right) \Big/ \left(1 + \frac{\sigma^*_{i,j}\Delta t}{2\mu_{i,j}}\right) \tag{13}$$

$$D_b|_{i,j} = \left(\frac{\Delta t}{\mu_{i,j}\Delta}\right) \Big/ \left(1 + \frac{\sigma^*_{i,j}\Delta t}{2\mu_{i,j}}\right) \tag{14}$$

for which $\Delta x = \Delta y = \Delta$ is assumed.

An expression for the magnetisation vector components can be obtained by expanding the vector product in LLG equation (7) and solving for $\partial M_x/\partial t$, $\partial M_y/\partial t$ and $\partial M_z/\partial t$; this yields

$$\begin{aligned}\frac{\partial M_x}{\partial t} &= \frac{\gamma}{M_s(1+\alpha^2)}[M_s(H_z M_y - H_y M_z) \\ &+\alpha M_x(H_y M_y + H_z M_z) - \alpha H_x(M_s^2 - M_x^2)]\end{aligned} \tag{15}$$

$$\begin{aligned}\frac{\partial M_y}{\partial t} &= \frac{\gamma}{M_s(1+\alpha^2)}[M_s(H_x M_z - H_z M_x) \\ &+\alpha M_y(H_x M_x + H_z M_z) - \alpha H_y(M_s^2 - M_y^2)]\end{aligned} \tag{16}$$

$$\begin{aligned}\frac{\partial M_z}{\partial t} &= \frac{\gamma}{M_s(1+\alpha^2)}[M_s(H_y M_x - H_x M_y) \\ &+\alpha M_z(H_x M_x + H_y M_y) - \alpha H_z(M_s^2 - M_z^2)]\end{aligned} \tag{17}$$

Applying central time differences to (15) and evaluating M_x at time step $n + 1/2$ yields

$$\frac{M_x|^{n+1} - M_x|^n}{\Delta t} = f(H_x, H_y, H_z, M_x, M_y, M_z)|^{n+\frac{1}{2}} \tag{18}$$

rearranging terms gives the time marching scheme for M_x

$$M_x|^{n+1} = M_x|^n + f(H_x, H_y, H_z, M_x, M_y, M_z)|^{n+\frac{1}{2}}\Delta t \tag{19}$$

where $f(H_x, H_y, H_z, M_x, M_y, M_z)$ is a function of the magnetic field and the magnetisation vector components coming from (15) and has the form

$$\begin{aligned}f(H, M) = \frac{\gamma}{M_s(1+\alpha^2)}\Bigg[& M_s(H_z M_y - H_y M_z) \\ &+\alpha M_x(H_y M_y + H_z M_z) - \alpha H_x \frac{M_s^2 - M_x^2}{M_y^2 + M_z^2}\Bigg]\end{aligned} \tag{20}$$

The magnetisation components are evaluated at the same spatial location as the magnetic field components in the Yee's cell. Time marching expressions for M_y and M_z are derived in the same manner. From equation (19) it is noticed that M_y, M_z, H_y and H_z are used to compute the new value of M_x, however, these are placed at different locations than M_x within the Yee's cell, therefore spacial interpolation is needed. It is also noticed that equation (19) uses M_x, M_y, M_z, H_x, H_y and H_z evaluated at time step $n + 1/2$ while their values are only known at time step n, with n being an integer, thus time extrapolation is required. The proper space and time discretisation of LLG equation to maintain second order accuracy are addressed in detail next.

IV. Space and Time Synchronism

Here two different problems are addressed to maintain second order accuracy of the central difference scheme. First, H_x, H_y, H_z, M_x, M_y and M_z are not known at time step $n+1/2$ in (19) or any other M (the same applies for the time marching expressions for M_y and M_z). A simple approach to solve this problem is to use an extrapolation scheme [15] in which the current value of a variable depends on the previous values using the backward differencing approximation

$$u|^{n+\frac{1}{2}} \simeq u|^{n-\frac{1}{2}} + \left.\frac{\partial u}{\partial t}\right|^{n-\frac{1}{2}} \Delta t \tag{21}$$

The unknown value of $u|^{n-\frac{1}{2}}$ on the right side of the equation can be expressed as the average of $u|^{n-1}$ and $u|^n$ and the derivative can be estimated using standard central differences. These operations lead to the second order accurate time marching formalism for correct integration into the FDTD scheme.

$$\begin{aligned}u|^{n+\frac{1}{2}} &\simeq \tfrac{u|^{n-1}+u|^n}{2} + u|^n - u|^{n-1} \\ &= \tfrac{1}{2}(3u|^n - u|^{n-1})\end{aligned} \tag{22}$$

To illustrate the time synchronism, M_x will be computed for time step $n + 1$. From (19), H_x, H_y, H_z, M_x, M_y and M_z must be known at time step $n + 1/2$ in order to evaluate $M_x|^{n+1}$. This is done by applying the time synchronism equation (22) to all vector components of $\mathbf{H}$ and $\mathbf{M}$ using previous values at time steps n and $n - 1$.

$$H_{x,y,z}|^{n+\frac{1}{2}} = \frac{1}{2}(3H_{x,y,z}|^n - H_{x,y,z}|^{n-1}) \tag{23}$$

$$M_{x,y,z}|^{n+\frac{1}{2}} = \frac{1}{2}(3M_{x,y,z}|^n - M_{x,y,z}|^{n-1}) \tag{24}$$

Now, all components on the right side of equations (23) and (24) are known, however, it is not yet possible to compute the magnetisation vector at time step $n + 1$ in the time marching scheme because space synchronism has not been applied.

In the Yee's cell, the $\mathbf{M}$ components are evaluated at the same spatial location as the $\mathbf{H}$ components. Therefore when any component of the magnetisation vector say M_x is being computed at a given point, say $(i + \frac{1}{2}, j)$, the y and z components of $\mathbf{H}$ and $\mathbf{M}$ used to compute $\mathbf{M_x}$ are located at different space locations as shown in Figure 1.

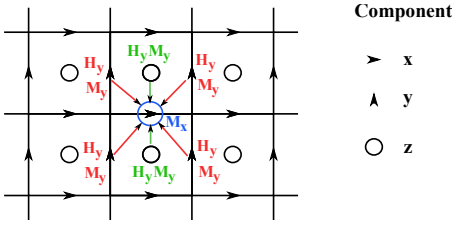

Fig. 1. Reallocation of components in a 2D Yee's cell for space synchronisation.

Thus, all the components in equations (23) and (24) must be reallocated to M_x position. This is done by interpolation of all components surrounding M_x in the Yee's cell [15]. This can be easy understood by a graphical example. Figure 1 represents the space synchronism operations needed to compute M_x (blue circle) where M_y at spatial point $(i+\frac{1}{2}, j)$ will be the average of the four M_y components surrounding Mx in Figure 1. This is the operation represented by the red arrows denoted below as $M_y\_M_x$.

$$M_y\_M_x|_{i+\frac{1}{2},j}^{n+\frac{1}{2}} = \frac{1}{4}\left(M_y|_{i,j-\frac{1}{2}}^{n+\frac{1}{2}} + M_y|_{i,j+\frac{1}{2}}^{n+\frac{1}{2}} + M_y|_{i+1,j-\frac{1}{2}}^{n+\frac{1}{2}} + M_y|_{i+1,j+\frac{1}{2}}^{n+\frac{1}{2}}\right) \quad (25)$$

The same must be done with $H_y\_M_x$ (red arrows operation)

$$H_y\_M_x|_{i+\frac{1}{2},j}^{n+\frac{1}{2}} = \frac{1}{4}\left(H_y|_{i,j-\frac{1}{2}}^{n+\frac{1}{2}} + H_y|_{i,j+\frac{1}{2}}^{n+\frac{1}{2}} + H_y|_{i+1,j-\frac{1}{2}}^{n+\frac{1}{2}} + H_y|_{i+1,j+\frac{1}{2}}^{n+\frac{1}{2}}\right) \quad (26)$$

In a similar way $M_z\_M_x$ (M_z to compute M_x) is described by the operation represented by green arrows.

$$M_z\_M_x|_{i+\frac{1}{2},j}^{n+\frac{1}{2}} = \frac{M_z|_{i+\frac{1}{2},j-\frac{1}{2}}^{n+\frac{1}{2}} + M_z|_{i+\frac{1}{2},j-\frac{1}{2}}^{n+\frac{1}{2}}}{2} \quad (27)$$

The same must be done with $H_z\_M_x$ if any (green arrows operation).

$$H_z\_M_x|_{i+\frac{1}{2},j}^{n+\frac{1}{2}} = \frac{H_z|_{i+\frac{1}{2},j-\frac{1}{2}}^{n+\frac{1}{2}} + H_z|_{i+\frac{1}{2},j-\frac{1}{2}}^{n+\frac{1}{2}}}{2} \quad (28)$$

H_x and M_x to compute M_x will remain the same as they are already in the same spatial position as M_x.

$$M_x\_M_x|_{i+\frac{1}{2},j}^{n+\frac{1}{2}} = M_x|_{i+\frac{1}{2},j}^{n+\frac{1}{2}} \quad (29)$$

$$H_x\_M_x|_{i+\frac{1}{2},j}^{n+\frac{1}{2}} = H_x|_{i+\frac{1}{2},j}^{n+\frac{1}{2}} \quad (30)$$

Then the values obtained from (25) to (30) are used in (20) to calculate $f(H_x, H_y, H_z, M_x, M_y, M_z)$ at time step $n+1/2$. To finish the computation of $M_x|^{n+1}$ the previous result and the known value of M_x at time n are introduced in (19).

The purpose of all these operations referred here as space and time synchronism is to maintain the second order accuracy in the differentiating scheme.

V. Boundary Conditions

From the minimisation of the total energy in a magnetic material, the following boundary condition is derived [16], [17]:

$$\frac{\partial \mathbf{M}}{\partial \mathbf{n}} = 0 \quad (31)$$

where $\mathbf{n}$ is the direction normal to the material surface. For example, solving (31) at the left boundary of the material ($n = -x$) involves the following operations

$$M_x|_{i+\frac{1}{2}} = M_x|_{i+\frac{3}{2}} \quad (32)$$

$$M_y|_i = M_y|_{i+1} \quad (33)$$

$$M_z|_{i+\frac{1}{2}} = M_z|_{i+\frac{3}{2}} \quad (34)$$

and similar equations would apply for other directions of $\mathbf{n}$.

The perfectly matched layer (PML) around the computational space used in normal FDTD to absorb the outgoing waves can be used for the extended method as far as the magnetic material is surrounded by the computational space and not in contact with the PML areas. This is based on the fact that the magnetisation vector has zero value outside the material (it doesn't exist) therefore the extended equations without the magnetisation are the same as in the normal FDTD method.

VI. Stability of the Extended Method

Due to the rotation of the magnetisation in a magnetic material another upper limit in Δt must be considered to make a stable solution for LLG equation. The worst case happens when damping is neglected and a strong field is applied in one direction, therefore the magnetisation describes a circular movement perpendicular to the applied field with a precession angular frequency $\omega_0 = \gamma H$ which in this particular case will be equal to the maximum rotational angular frequency of the magnetisation. Then, the equation of

motion can be written as:

$$\left.\begin{aligned}\frac{dM_x}{dt} &= \omega_0 M_y \\ \frac{dM_y}{dt} &= -\omega_0 M_x \\ \frac{dM_z}{dt} &= 0\end{aligned}\right\} \tag{35}$$

In order to obtain an equation explicitly for, say M_x, expression (35) must be differentiated to give:

$$\frac{d^2 M_x}{dt^2} = \omega_0 \frac{dM_y}{dt} \tag{36}$$

Substituting dM_y/dt from (35) into (36) yields the ordinary differential equation for M_x:

$$\frac{d^2 M_x}{dt^2} = -\omega_0^2 M_x \tag{37}$$

Applying central finite differences to this equation:

$$\frac{M_x^{n+1} - 2M_x^n + M_x^{n-1}}{(\Delta t)^2} = -\omega_0^2 M_x^n \tag{38}$$

and solving for M_x^{n+1} yields the explicit time marching scheme for M_x

$$\begin{aligned} M_x^{n+1} &= 2M_x^n - M_x^{n-1} - \omega_0^2 \Delta t^2 M_x^n \\ &= M_x^n (2 - \omega_0^2 \Delta t^2) - M_x^{n-1} \end{aligned} \tag{39}$$

Using a complex exponential solution $M_x = M_s e^{j\omega_0 t}$ and substituting in (39) gives

$$e^{j\omega_0 (n+1)\Delta t} = e^{j\omega_0 n \Delta t}(2 - \omega_0^2 \Delta t^2) - e^{j\omega_0 (n-1)\Delta t} \tag{40}$$

Expanding the exponential terms and applying Euler's relation to the exponential terms gives

$$2\cos(\omega_0 \Delta t) = 2 - \omega_0^2 \Delta t^2 \tag{41}$$

Equation (41) relates the angular frequency of the system to the time increment. Furthermore

$$\omega_0 \Delta t = \cos^{-1}\left(1 - \frac{\omega_0^2 \Delta t^2}{2}\right) = \cos^{-1}\xi \tag{42}$$

As in the general case for non-magnetic materials, stability is found for the values of ξ that make $\omega_0 \Delta t$ in equation (42) to be real. For values of ξ outside the interval -1 and 1, the function $\cos^{-1}\xi$ will be complex valued and therefore the rotation of magnetisation will produce an unstable solution. At the limits of the above interval

$$\xi = 1 - \frac{\omega_0^2 \Delta t^2}{2} = 1 \quad \rightarrow \quad \Delta t = 0 \tag{43}$$

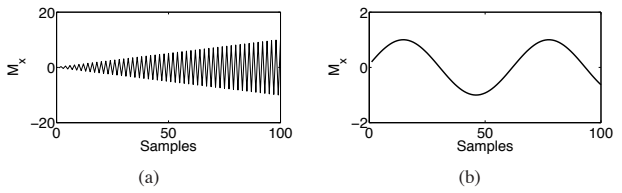

Fig. 2. Solution of (37) sampled with (a) $\Delta t = 2/\omega_0$ which makes the system unstable and (b) $\Delta t = 0.1/\omega_0$ which makes the system stable.

$$\xi = 1 - \frac{\omega_0^2 \Delta t^2}{2} = -1 \quad \rightarrow \quad \Delta t = \frac{2}{\omega_0} \tag{44}$$

Therefore defining the range of Δt for the stable solution of the oscillator equation (37)

$$0 < \Delta t < \frac{2}{\omega_0} = UpperBound \tag{45}$$

This is clearly understood by an example. Figure 2(a) represents a sampled solution of (37) with a sampling rate of $\Delta t = 2/\omega_0$ which is just over the limit in (45) therefore the system is unstable and the solution grows to infinity as time goes on. Figure 2(b) is an example of a stable solution where $\Delta t = 0.1/\omega_0$ implies a stable solution. Although equation (45) defines the stable range when the magnetisation is introduced, the general equation that rules the stability of the FDTD method still needs to be considered as

$$\Delta t > 1 \Big/ c\sqrt{\tfrac{1}{(\Delta x)^2} + \tfrac{1}{(\Delta y)^2}} \equiv \Delta t_{stable\ limit_{2D}} \tag{46}$$

Therefore the time increment of the system Δt must be bounded in such a way that satisfies both (45) and (46) to avoid instability.

To finalise with the stability section, the solution to LLG equation is convergent when the magnetisation is aligned with the applied field or expressed mathematically as

$$\frac{|\mathbf{M} \times \mathbf{H}|}{|\mathbf{M}| \cdot |\mathbf{H}|} \approx 1 \tag{47}$$

This then provides a test of convergence in the numerical implementation.

VII. Experiment Set Up and Results

Figure 3 represents the head diagram used for the simulations. Both geometry and dimensions were taken from an actual Seagate head manufactured in 1997 trhough electron microscope imaging. Two snapshots of the magnetic field strength during simulation

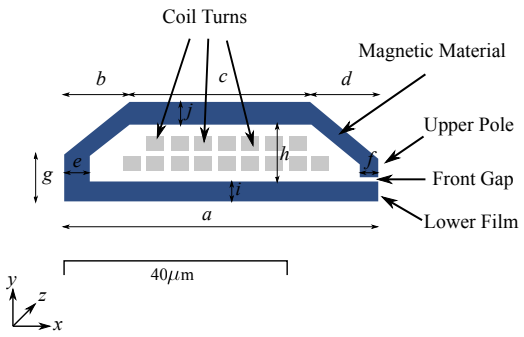

Fig. 3. Scaled diagram of the head geometry with dimensions: front gap height= 0.5μm, a= 56.7μm, b= 11.5μm, c= 33.3μm, d= 11.9μm, e= 4.6μm, f= 2.7μm, g= 10.2μm, h= 12.4μm, i= 4.6μm, j= 4.6μm. For simulation purposes the axis are taken as shown where the z-axis represents the anisotropy axis.

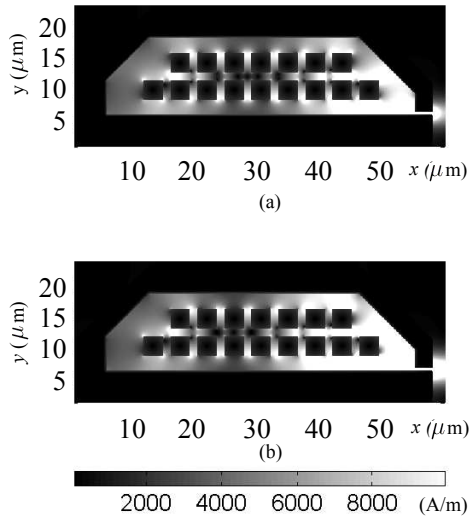

Fig. 4. Magnetic field magnitude for two time instants, (a) $t = 0.2$ns and (b) $t = 0.45$ns, computed using the standard FDTD algorithm (no magnetisation is considered) and a 15mA current step excitation with rise time constant 20ps.

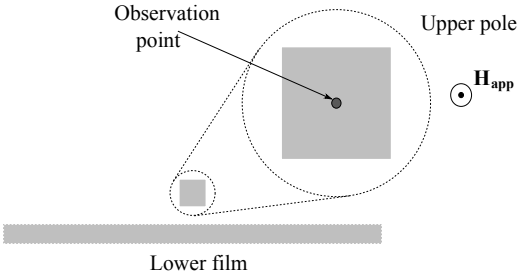

Fig. 5. Configuration of the upper pole simulation in the TE_z mode. Only the zoomed image of the upper pole is defined in the simulation. The excitation is applied uniformly as indicated by $\mathbf{H_{app}}$.

in the TMz mode are shown in Figure 4. Figure 5 represents the configuration used to carry out simulations of the upper pole of head A in TEz mode. These were aimed to study the effects of eddy currents on the switching time due to a field step applied perpendicular to the plane of the paper, with 20ps time constant and 12×10^3A/m amplitude. The simulation parameters were $\Delta x = 0.5\mu$m, $\Delta t = 0.83333$fs and total simulation time 1ns. With regards to material properties, three types of materials were considered: a perfect conductor for the coil turns, a magnetic material for the head core and an isolating material between them. The coil turns were defined by a conductivity $\sigma = 5.8 \times 10^7$ (1/Ωm) and a relative permittivity $\epsilon_r = 4.8$; The magnetic material was defined by a low electrical conductivity $\sigma = 5000$ (1/Ωm), saturation magnetisation $M_s = 800 \times 10^3$ (A/m) initially oriented in the y direction, damping coefficient $\alpha = 0.1$ (μm), uniaxial anisotropy with $H_k = 400$ (A/m) and anisotropy constant $K_u = 200$ (J/m^3), and exchange stiffness constant $A_x = 1.0 \times 10^{-11}$ (J/m); The isolating material was defined by $\epsilon_r = 1$, $\mu_r = 1$ and $\sigma = 0$. Demagnetising fields were included as another term in the direction of the applied field into the effective field expression. Considering the head pole as an infinite cylinder, the demagnetising energy can be expressed as

$$\mathcal{E}_{demag} = \frac{\mu_0}{2}(N_x M_x^2 + N_y M_y^2 + N_z M_z^2) \qquad (48)$$

where due to the cylindrical geometry and orientation in the z direction, $N_x = N_y = 1/2$ and $N_z = 0$. Then

$$\mathcal{E}_{demag} = \frac{\mu_0}{2}\left(\frac{M_x^2}{2} + \frac{M_y^2}{2}\right) \qquad (49)$$

The applied energy can be expressed as

$$\mathcal{E}_h = -\mu_0 \mathbf{M}\mathbf{H_{app}} \qquad (50)$$

where $\mathbf{H_{app}} = H_z\mathbf{k}$, then

$$\mathcal{E}_h = -\mu_0 M_z H_z \qquad (51)$$

Now, considering the total free energy as the applied and demagnetising field contributions

$$\mathcal{E}(\mathbf{M}) = \frac{\mu_0}{2}\left(\frac{M_x^2}{2} + \frac{M_y^2}{2}\right) - \mu_0 M_z H_z \qquad (52)$$

or by normalising by $\mu_0 M_s$

$$\hat{\mathcal{E}}(\mathbf{m}) = \frac{1}{4}(m_x^2 + m_y^2) - m_z h_z \qquad (53)$$

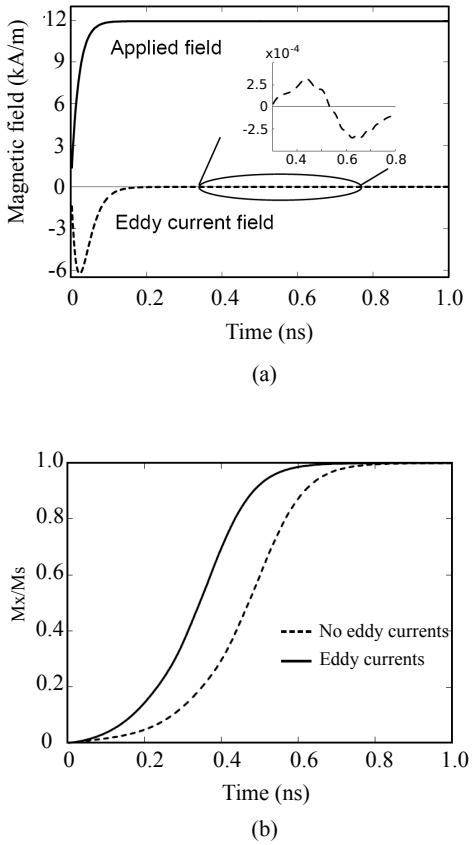

Fig. 6. Eddy current effect at the head pole. (a) Applied field and corresponding eddy current field. (b) Out of plane magnetisation versus time showing a 0.13ns delay in the precessional switching of the magnetisation.

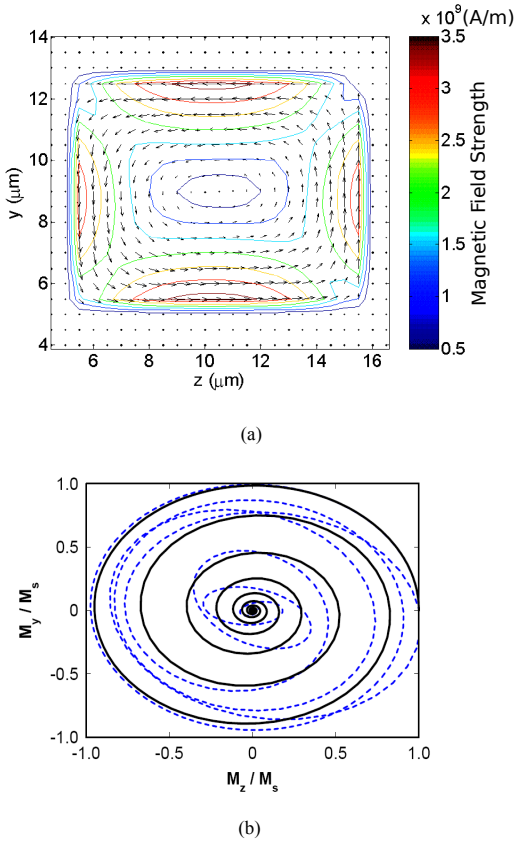

Fig. 7. Eddy current effect at the head pole. (a) Contour and arrow plot of the current density (A/m^2) at 0.02ns. (b) Magnetisation precession with (dashed plot) and without (solid plot) eddy current fields.

Since $m_x^2 + m_y^2 + m_z^2 = 1$, then

$$\hat{\mathcal{E}}(\mathbf{m}) = \frac{1}{4}(1 - m_z^2) - m_z h_z \tag{54}$$

which concludes with effective field expression as

$$\mathbf{h_{eff}} = -\frac{\partial \hat{\mathcal{E}}}{\partial \mathbf{m}} = \left(\frac{m_z}{2} + hz\right)\mathbf{k} \tag{55}$$

The magnetic fields and the magnetisation were evaluated at the center of the head pole. Figure 6(a) shows that eddy currents produce opposing fields to the applied field that turns out to trigger the precessional switching of the magnetisation. Analysing the plot in Figure 6(b), when eddy currents are not considered, a delay of 0.13ns is observed in the switching time of the magnetisation, which causes a slower head field response in agreement with the literature. The expanded plot in Figure 6(a) represents eddy current field due to $\partial M/\partial t$ which is negligible. Figure 7(a) shows the current density across the head pole, its distribution agrees with the theory of eddy currents that can be found in the literature. The eddy current fields trigger the switching of the magnetisation and also modify its precession as can be seen in Figure 7(b).

Figure 8 shows the magnetic field distribution near the gap region at time 0.45ns for both the standard and the extended FDTD algorithms. By comparison, it is observed that when using the extended method, the field strength is smaller and the effective field concentrates at the head corners. As explained above, these effects are due to the switching of the magnetisation and the demagnetising fields. The arrow plot of Figure 8(b) represents the orientation of the magnetisation. The direction of the magnetic flux density can be visualised by observing the orientation of the magnetisation arrows, it is obvious that there is a flux linking both thin films through the gap resulting in the external radiation of the write field.

Figure 9 is obtained by plotting the magnetic field

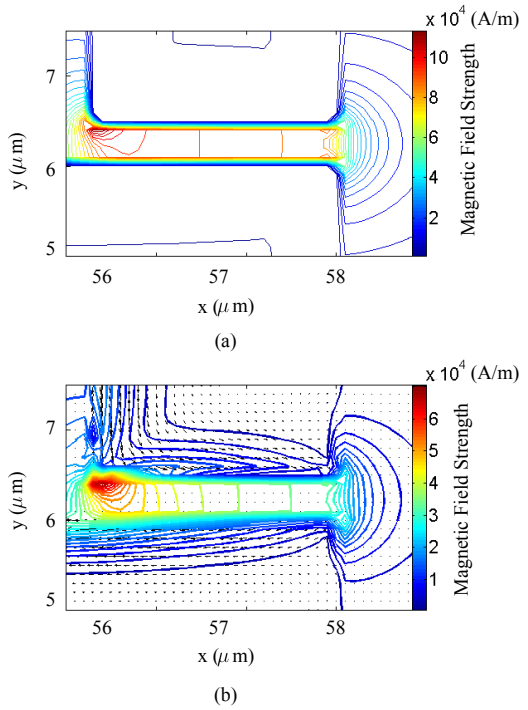

Fig. 8. Magnetic field distribution of the head geometry near the gap region at simulation time 0.45ns. (a) Contour plot of the field strength for linear material and (b) contour plot of the field strength and arrow plot of the magnetisation for non-linear material.

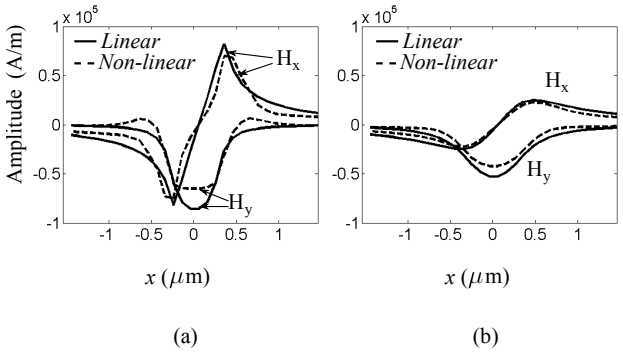

Fig. 9. Recording gap fields simulating a plane parallel to the disk surface in a recording system. (a) Fields at the pole surface and (b) at 100nm from the head surface.

components H_x and H_y at the head surface and at a distance of 100nm from the head surface in the gap region. Here, the x-axis represents distances from the central point of the gap region towards both poles (upper and lower), e.g. $x = 0$ is the value taken in the centre of the gap at a distance of 100nm away from the head, the direction of x is parallel to the disk surface. Having in mind that the disk surface in a recording system would be parallel to this plane, the field magnitude responsible for orientating the magnetisation of the disk in one direction or another will be proportional to the plot in Figure 9. In particular, H_y is the main field responsible for the recording process in longitudinal media. Higher field gradients are observed in the pole corner regions with the inclusion of the magnetic details of the core material. This has the implication that shorter transition lengths are recorded in practice than predicted by models that ignore the magnetic detail of the core material.

The obtained results are in agreement with previous works present in the literature. In [18], a similar delay of 0.25ns was observed when considering a damping coefficient $\alpha = 0.1$, which triggers the precession of the magnetisation. The same conclusions were drawn in [19] with respect to the precession of the magnetisation: eddy currents introduce an eddy current field that triggers the precession. In [20], a faster magnetisation switching was also observed, it was triggered by the eddy currents which turned out into a slower head field response. In [21], authors agree with the fact that the effect of eddy currents is completely different when considering micromagnetic level models and thus the effect of the magnetisation can not be represented by an equivalent permeability. Also, predicted gap field distributions showed a more accurate field description near the head poles when compared against simpler head models, e.g. Karlqvist [22].

Regarding the memory requirement, in order to store each sample, the extended FDTD simulation requires 153,558,419 bytes, figure which is, without surprise, above the amount of memory that uses the standard FDTD method to simulate the same head structure, 26,345,603 bytes. With respect to the calculation time, the time increment in between consecutive iterations of an FDTD execution is directly related to the spatial resolution of the grid in the FDTD algorithm, stability equations (45) and (46). The grid resolution is determined by the most restrictive of two factors: the smallest feature in the simulated structure or the shortest wavelength in the simulated space. In this particular case, where a magnetic head has been simulated, the very small front gap height for the head geometry in Figure 3 determined a very small time increment resulting in a large number of iterations. Thus, a small grid resolution results in a very small time increment and therefore large simulation time (CPU time) to obtain the results of a single simulation

(the TM_z Matlab simulation took fifty days overall on a 2GHz machine, with 2GB of RAM, running on Windows XP). Large waiting time requirements have made it impossible to carry out several simulations and other tests over very small head structures.

VIII. Conclusion

This investigation aimed at developing a numerical simulation approach that simultaneously incorporates the fundamental micromagnetic and electromagnetic details of magnetic materials to study the fast switching process in soft magnetic materials in general, and in thin-film inductive writers in particular.

This work successfully met all its original objectives by developing a numerical technique for simulating the dynamic behaviour of magnetic materials and devices. This technique naturally combines the fundamental equation of magnetisation motion with the solution of Maxwell's equations using the Finite- Difference Time-Domain method, with the unique feature that the micromagnetic (including exchange and anisotropy effects) and electromagnetic (electric and magnetic fields due to charges and currents) descriptions of simulated structures are produced simultaneously.

Using this technique will help to design and study complete magnetic devices without ignoring the interaction between the magnetic material and other dielectric and conductive layers in the structure, which is important at high frequencies. Moreover, this feature simplifies the magnetostatic computations which are inherently demanding in numerical micromagnetics, thus extending existing work in micromagnetics to more complex geometries and applications.

References

[1] R. J. Hicken, N. D. Hughes, J. R. Moore, D. S. Schmool, and J. W. R. Wilks, "Magneto-optical studies of magnetism on pico and femtosecond time scales," *Journal of Magnetism and Magnetic Materials*, vol. 242-245, no. 1, pp. 559–564, 2002.

[2] C. H. Back, J. Heidmann, and J. M. Cord, "Time resolvel kerr microscopy: Magnetisation dynamics in thin film write heads," *Magnetics, IEEE Transactions on*, vol. 35, pp. 637–642, 1999.

[3] B. K. Middleton, J. J. Miles, and M. M. Aziz, "Switching times and transition widths in digital recording theory," *Magnetics, IEEE Transactions on*, vol. 37, pp. 1327–1329, 2001.

[4] I. Tagawa, T. Koshikawa, and Y. Sasaki, "High performance write head for 10 krpm hdd with high data rate recording up to 45 mb/s," *Magnetics, IEEE Transactions on*, vol. 36, no. 1, pp. 177–182, 2000.

[5] G. Rubinacci, A. Tamburrino, and S. Ventre, "Eddy Current Imaging of Surface Breaking Defects by Using Monotonicity Based Methods," *Applied Computational Electromagnetics Society (ACES) Journal*, vol. 23, no. 1, pp. 46–52, 2008.

[6] H. Engstrom, "Equivalent circuit of a thin film recording head," *Magnetics, IEEE Transactions on*, vol. 20, no. 5, pp. 842–844, 1984.

[7] A. Paton, "Analysis of the efficiency of thin film magnetic recording heads," *J. Appl. Phys.*, vol. 42, no. 13, pp. 5868–5870, 1971.

[8] R. E. Jones, "Analysis of the efficiency and inductance of multiturn thin film magnetic recording heads," *Magnetics, IEEE Transactions on*, vol. 14, no. 5, pp. 509–511, 1978.

[9] T. Arnoldussen, "A modular transmission line/reluctance head model," *Magnetics, IEEE Transactions on*, vol. 24, no. 6, pp. 2482–2484, 1988.

[10] N. Yeh, "Analysis of thin film head with a generalized transmission line model," *Magnetics, IEEE Transactions on*, vol. 18, no. 1, pp. 233–237, 1982.

[11] F. Liu, S. Shi, J. Wang, Y. Chen, K. Stoev, L. Leal, R. Saha, H. Tong, S. Dey, and M. Nojaba, "Magnetic recording at a data rate of one gigabit per second," *Magnetics, IEEE Transactions on*, vol. 37, no. 2, pp. 613–618, 2001.

[12] K. Gao and H. N. Bertram, "Three dimensional micromagnetic analysis of write head dynamics and field patterns," *Magnetics, IEEE Transactions on*, vol. 37, no. 4, pp. 1373–1375, 2001.

[13] S. Hagness and A. Taflove, *Computational Electrodynamics, the Finite Difference Time Domain Method*. Artech House, 2000.

[14] T. L. Gilbert, "A lagrangian formulation of the gyromagnetic equation of the magnetic field," *Physical Review*, vol. 100, 1955.

[15] M. Okoniewski and E. Okoniewska, "FDTD analysis of magnetized ferrites: a more efficient algorithm," *Microwave and Guided Wave Letters, IEEE*, vol. 4, no. 6, pp. 169–171, 1994.

[16] W. F. Brown, *Micromagnetics*. Robert E. Krieger publishing company Huntington, New York, 1978.

[17] A. Aharoni, *Introduction to the Theory of Ferromagnetism*. Oxford Science Publications, 2nd ed., 2000.

[18] L. Torres, L. Lopez-Diaz, E. Martinez, and O. Alejos, "Micromagnetic dynamic computations including eddy currents," *Magnetics, IEEE Transactions on*, vol. 39, pp. 2498 – 2500, sept. 2003.

[19] G. Hrkac, T. Schrefl, O. Ertl, D. Suess, M. Kirschner, F. Dorfbauer, and J. Fidler, "Influence of eddy current on magnetization processes in submicrometer permalloy structures," *Magnetics, IEEE Transactions on*, vol. 41, pp. 3097 – 3099, oct. 2005.

[20] K. Takano, X. Zhang, E.-A. Salhi, L. Guan, M. Sakai, J. Smyth, and M. Dovek, "Micromagnetics and eddy current effects in magnetic recording heads," *Magnetics, IEEE Transactions on*, vol. 43, pp. 2184 –2186, june 2007.

[21] E. Della Torre and J. Eicke, "Eddy currents in micromagnetic calculations," *Magnetics, IEEE Transactions on*, vol. 33, pp. 1251 –1254, mar 1997.

[22] O. Karlqvist, "Calculation of the magnetic field in the ferromagnetic layer of a magnetic drum," *Trans. Roy. Inst. Techno., Stockholm*, no. 86, pp. 3 –27, 1954.